

# Analysis of the Spontaneous Emission Limited Linewidth of an Integrated III–V/SiN Laser

Weng W. Chow, Yating Wan,\* John E. Bowers, and Frédéric Grillot

This article describes a calculation of the spontaneous emission limited linewidth of a semiconductor laser consisting of hybrid or heterogeneously integrated, silicon and III–V intracavity components. Central to the approach are a) description of the multi-element laser cavity in terms of composite laser/free-space eigenmodes, b) use of multimode laser theory to treat mode competition and multiwave mixing, and c) incorporation of quantum-optical contributions to account for spontaneous emission effects. Application of the model is illustrated for the case of linewidth narrowing in an InAs quantum-dot laser coupled to a high- $Q$  SiN cavity.

obtained.<sup>[10]</sup> Further improvement was achieved with a hybrid integrated laser that included a commercial DFB laser butt-coupled to the bus waveguide of the Si<sub>3</sub>N<sub>4</sub> resonator chip.<sup>[11]</sup> With a high cavity  $Q > 2.5 \times 10^8$ , an electrically pumped integrated laser with a linewidth of 1.2 Hz was demonstrated.

This paper describes a calculation of the spontaneous emission limited spectrum of a semiconductor laser consisting of III–V and SiN sections. A composite-cavity mode description is used to treat the effects of optical coupling among different intracavity components in an

## 1. Introduction

For coherent communication and sensing, there is much effort toward developing narrow linewidth semiconductor lasers, beyond what is achievable with single Fabry-Perot or distributed feedback (DFB) resonators.<sup>[1]</sup> To reduce spectral linewidth, many approaches are being considered, including external cavity, phase-shifted and chirped grating, discrete mode DFB lasers, and fiber lasers.<sup>[2–6]</sup> From the active region aspect, InAs/InP quantum dot (QD) DFB lasers, operating with very low population inversion, have achieved spectral linewidth down to 30 kHz.<sup>[7,8]</sup> Recently, much progress is reported on modal engineering of a DFB laser, in which light is generated in the III–V material and stored into the low-loss silicon material. This class of hybrid or heterogeneous integrated lasers indicates a promising path forward, where wavelengths down to 1 kHz level have already been demonstrated.<sup>[9]</sup> The laser structure relies on using a harmonic potential cavity to produce a large quality factor ( $Q$ ). A similar design has been proposed and a long photon lifetime of 103 ps was


extended cavity.<sup>[12]</sup> The composite-cavity modes also provide a treatment of outcoupling that is more consistent with mode projections used in laser theory.<sup>[13,14]</sup> Active medium contributions are described within the context of multimode semiclassical laser theory, where electron–hole polarization dynamics accounts for both linear gain and carrier-induced refractive index change, as well as nonlinearities giving rise to saturation, mode competition and multiwave mixing.<sup>[14]</sup> Strictly speaking, the intrinsic linewidth determination requires radiation field quantization. We have taken such an approach in the past and found the numerical evaluation of the two-time field correlations to be very demanding, especially for parametric studies involving complex resonators and accounting for multimode effects.<sup>[15]</sup> Instead, we extracted from the single-mode quantum-optical derivation, terms arising from spontaneous emission that can be incorporated into the intensity and frequency determining equations in laser theory. Our approach resembles a Langevin description<sup>[16]</sup> with the added complication of a complex resonator geometry and a more consistent treatment of outcoupling.

Section 2 describes the formulation of the approach. The concept of composite-cavity modes is discussed, along with their advantages, in terms of validity for arbitrary coupling between III–V and SiN sections, and a consistent treatment of laser outcoupling. Also, the section describes the use of composite-cavity modes in a multimode semiconductor-laser theory to account for active region contributions. The section ends with a discussion on the incorporation of spontaneous emission contributions into the laser equations. Section 3 demonstrates the application of the approach to identify and understand the physical mechanisms leading to spectral narrowing in an extended cavity with III–V active and SiN passive sections. Results are discussed, that are from a parametric study involving the lasing linewidth dependences on the SiN cavity  $Q$  and the coupling between III–V and SiN sections.

W. W. Chow  
Sandia National Laboratories  
Albuquerque, NM 87185-1086, USA

Y. Wan, J. E. Bowers  
Department of Electronic and Computer Engineering  
University of California – Santa Barbara  
Santa Barbara, CA 93106, USA  
E-mail: yatingwan@ucsb.edu

F. Grillot  
LTCI, Télécom Paris  
Institut Polytechnique de Paris  
Palaiseau 91120, France

 The ORCID identification number(s) for the author(s) of this article can be found under <https://doi.org/10.1002/lpor.202100620>

DOI: 10.1002/lpor.202100620

## 2. Theory

### 2.1. Composite-Cavity Modes

A difference in our approach is the treatment of the optically coupled III–V and SiN sections as a combined system. This composite-cavity treatment provides a description that is valid for arbitrary coupling (i.e., from completely isolated to totally coupled). Variations of this approach have been used to investigate cleaved-coupled-cavity lasers, photonic-crystal lasers and isolator-free, injection-locked lasers.<sup>[12,17–20]</sup>

Assuming that transverse and longitudinal spatial dependences of the intracavity field may be decoupled, we use the effective index method to reduce to a 1-dimensional geometry. Then, Maxwell's equations become

$$\left( \frac{\partial^2}{\partial z^2} + \frac{n^2(z)}{c^2} \frac{\partial^2}{\partial t^2} - \frac{\alpha(z)}{c} \frac{\partial}{\partial t} \right) E(z, t) = -\mu_0 \frac{\partial^2}{\partial t^2} P(z, t) \quad (1)$$

where  $E(z, t)$  is the radiation field,  $P(z, t)$  is the polarization representing the active medium,  $\alpha(z)$  describes the losses (such as intracavity absorption) at various locations,  $\mu_0$  and  $c$  are the permeability and speed of light in vacuum. In Equation (1),  $t$  is time and  $z$  is the position along the III–V and SiN cavity axis. The arrangement of intracavity optical components is described by the  $z$ -dependence of the effective refractive index  $n(z)$ . Setting  $\delta^2 P / \partial t^2 = \alpha = 0$  and writing:

$$E(z, t) = E_m(t) \cos(v_m t) u_m(z) \quad (2)$$

we obtain the equation for a composite passive cavity eigenmode:

$$\frac{d^2}{dz^2} u_m(z) = \frac{n^2(z)}{c^2} \Omega_m^2 u_m(z) \quad (3)$$

where  $m$  is the mode index and  $\Omega_m$  is the eigenfrequency.

We also use the composite-cavity modes to circumvent an inconsistency in laser physics involving the treatment of the active medium and optical resonator contributions.<sup>[13,14]</sup> In laser theory, passive-cavity normal modes are necessary for performing the projections leading to the laser field amplitude- and frequency-determining equations. However, the rigorous definition of normal modes for a laser cavity is not possible because of mirror outcoupling. One customarily uses a set of quasi modes obtained from, e.g., a Fox-Li calculation, and accounts for cavity losses by adding a decay term to the amplitude-determining equation. Such a phenomenological approach is inadequate for describing the finer details of laser linewidth, such as the evolution of the emission spectrum during the transition from below to above lasing threshold. Instead, we follow an earlier paper treating outcoupling in a Fabry-Perot laser<sup>[21]</sup> by extending the effective refractive index  $n(z)$  in Equation (3) to include a very long resonator approximating free-space (see **Figure 1**).

Strictly speaking, Equation (3) should be solved using the precise  $n(z)$  describing the spatial variations in effective refractive index from the different material layers making up the distributed Bragg reflectors, spacer layers and waveguides. Such a detailed description is unnecessary as well as cumbersome for our present goal, which is a general understanding of the linewidth results when a laser is coupled to a very high- $Q$  passive

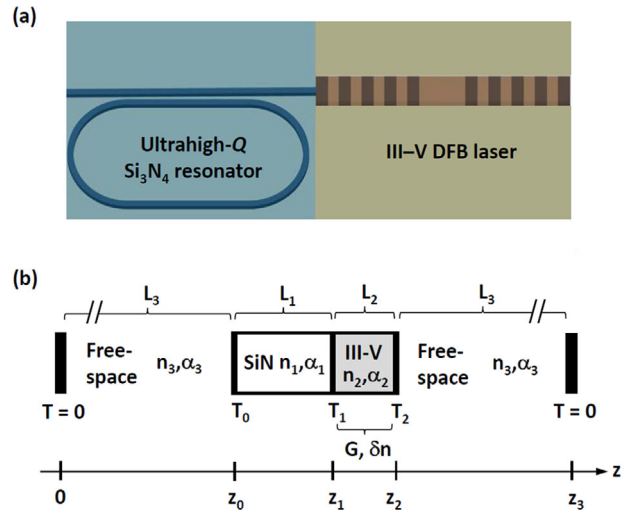


**Figure 1.** a) Sketch of an experimental laser operating with an extended cavity consisting of a high- $Q$  SiN resonator coupled to an III–V laser. b) Basic III–V/SiN coupled-cavity configuration used in the calculations. Input to the laser theory and connection to experimental devices such as in (a) are the passive cavity resonances. We specify them using the cavity lengths  $L_1$  and  $L_2$ , and transmissions  $T_0$ ,  $T_1$ , and  $T_2$ . The transmission  $T_1$  also approximates the effective coupling between SiN and III–V cavities, via either an index step, diffractive Bragg reflector (DBR) or evanescent field. The gain and carrier-induced refractive index ( $G$  and  $\delta n$ , respectively) are calculated from the laser theory.  $L_3$  is made sufficiently large to provide sufficient composite-cavity modes to accurately reproduce the finite-width (Fox-Li) resonances caused by outcoupling.

resonator. Hence, we will start with the basic 1-d geometry depicted in Figure 1b, where the interfaces between optical sections are treated by “bumps” in  $n(z)$ .<sup>[22]</sup> In this case, the composite-cavity modes have the boundary conditions:

$$u_m(0) = u_m(z_3) = 0 \quad (4)$$

$$u_m(z_i^+) = u_m(z_i^-) \quad (5)$$

$$\frac{d}{dz} u_m(z_i^+) - \frac{d}{dz} u_m(z_i^-) = -\eta_i k u_m(z_i) \quad (6)$$

where

$$\eta_i = 2\sqrt{\frac{(1 - T_i)}{T_i}} \quad (7)$$

$z_i^-$  and  $z_i^+$  are located immediately prior and after  $z_i$ ,  $T_i$  is the effective transmission representing the coupling between sections and  $k$  is the average magnitude of the wave vector. The orthogonality relation comes from integrating by parts Equation (3):

$$\int_0^{z_3} dz n^2(z) u_n(z) u_m(z) = \delta_{nm} N_c \quad (8)$$

where  $N_c = n_1^2 \times L_1 + n_2^2 \times L_2 + 2 \times n_3^2 \times L_3$  is the normalization.

To illustrate the basic properties of composite-cavity modes, we consider the example of two cavities of lengths and refractive indices  $L_1 = 4$  mm,  $n_1 = 2.1$  and  $L_2 = 600$   $\mu$ m,  $n_2 = 3.6$ . The

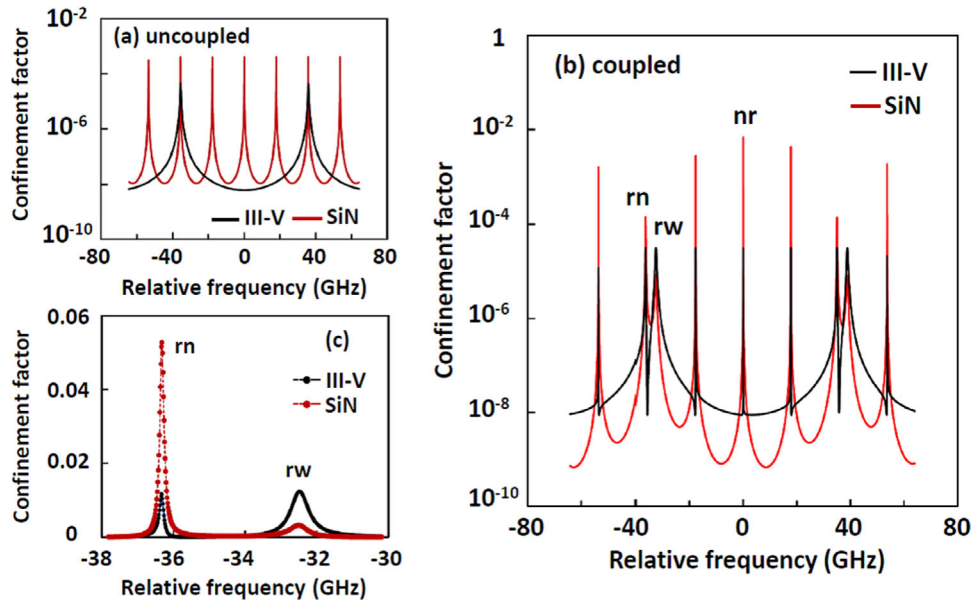


**Figure 2.** a) Resonances of individual III–V cavity (black) and SiN cavities (red). The frequency is relative to the central frequency of the composite-cavity modes used in the calculations. b) Resonances of the coupled system, in the III–V (black) and SiN cavities (red). The labels refer to resonances studied in the next section: resonant narrow (rn), resonant wide (rw), and non-resonant (nr). c) Higher resolution of double peak resonance within III–V cavity (black) and SiN cavity (red). Each composite mode contributes to a point in the resonances.

cavities are coupled via  $T_1 = 0.01$ , and the outcoupling is  $T_0 = 0$  and  $T_2 = 0.02$ . **Figure 2a** shows the plots of the resonances of the uncoupled III–V and SiN cavities, obtained by solving Equation (3). When coupled, the solution to Equation (3) gives the curves in **Figure 2b**. They show the resonances in the SiN and III–V cavities, specifically, the overlap of each composite-cavity mode within the two sections of the laser cavity:  $\Gamma_{1,m}^{(1)} = N_c^{-1} \int_{z_0}^{z_1} dz n_1^2 u_m^2(z)$  versus  $\Omega_m$  and  $\Gamma_{2,m}^{(1)} = N_c^{-1} \int_{z_1}^{z_2} dz n_2^2 u_m^2(z)$  versus  $\Omega_m$ . The magnitude of an integral gives of measure of the fraction of the mode residing in a particular section compared to in free space. The fraction,  $\Gamma_{2,m}^{(1)} / (\Gamma_{1,m}^{(1)} + \Gamma_{2,m}^{(1)})$  is the mode confinement factor typically present a laser gain formula derived with quasi-Fox-Li modes.

There are basically 3 kinds of resonances. Where the uncoupled III–V and SiN resonances coincide, **Figure 2b** shows two closely spaced composite-cavity resonances (rn and rw), with splitting determined by the coupling  $T_1$ . The other resonances (e.g., nr) belong to the eigenmodes of the longer SiN cavity. They also appear in the III–V cavity (black curve) because of cavity coupling.

Without coupling to free-space, the resonances in **Figure 2** would be delta functions. Outcoupling leads to finite-linewidth resonances (Fox-Li quasi modes) as depicted in **Figure 2c** for the resonant case. Each resonance is composed of multiple composite-cavity modes as indicated by the dots. Based on linewidths, one may associate the broad resonance (rw) with the III–V cavity, where cavity length  $L_2 = 600 \mu\text{m}$  and facet transmissions  $T_1 = 0.01$ ,  $T_2 = 0.02$  result in 550 MHz full-width at half-maximum (FWHM) and  $Q = 3.9 \times 10^5$ . The narrow resonance (rn) may be assigned to the SiN cavity, with length  $L_1 = 4 \text{ mm}$  and facet transmissions  $T_0 = 0$ ,  $T_1 = 0.01$  giving FWHM = 60 MHz

and  $Q = 3.6 \times 10^6$ . The red curve in **Figure 2c** for the SiN cavity also shows a weak, broad resonance injected from the III–V cavity. Similarly, the black curve in **Figure 2c** for the III–V cavity shows a narrow resonance injected from the SiN cavity. The difference in injection levels between the two cavities is because the SiN cavity high  $Q$  inhibits external influences, whereas the III–V cavity lower  $Q$  is less discriminating, hence, the non-reciprocity in mutual injection or self-feedback.

## 2.2. Laser Theory

To include the InAs QD active medium, we follow semiclassical laser theory<sup>[14]</sup> and write

$$P(z, t) = \frac{1}{2} \sum_n P_n(t) e^{-i[\nu_n t + \phi_n(t)]} u_n(z) + c.c. \quad (9)$$

where  $P_n(t)$  is the complex polarization amplitude. In Equation (9), the lasing frequency is usually written in two parts:  $\nu_n + d\phi_n/dt$ , where the large part  $\nu_n$  is typically,  $10^{14} \text{ s}^{-1}$  and the small part  $d\phi_n/dt$  is typically  $10^9 \text{ s}^{-1}$ . That  $\nu_n \gg d\phi_n/dt$  is used in the derivation of the laser frequency-determining equation. In addition, the slowly varying phase derivative  $d\phi_n/dt$  accounts for the active medium modifications to the passive cavity frequency  $\Omega_n$ . In semiclassical laser theory, the complex polarization amplitude connects Equation (1) to a quantum mechanical electron-hole polarization via

$$P_n(t) = 2 \frac{\mathcal{E} N_{QD}^{(2d)}}{h_{QW}} e^{i[\nu_n t + \phi_n(t)]} \frac{\Gamma_{xy}}{N_c} \int_{z_1}^{z_2} dz n^2(z) u_n(z) \sum_q \langle b_q(t) c_q(t) \rangle \quad (10)$$

**Table 1.** Active medium coefficients, where  $L_\gamma(x) = 1/[1 + (x/\gamma)^2]$ ,  $F_1 = \wp^2 v_0 N_{\text{QD}}^{(2d)} / (2\hbar\gamma\epsilon_B h_{\text{qw}})$  and  $D_\gamma(x) = 1/(1 + ix/\gamma)$ .

Parameter	Equation
Saturated gain	$g_n^{\text{sat}} = g_n / (1 + \sum_m \kappa_{nm} I_m)$
Linear gain and frequency pulling	$g_n/2 + i\sigma_n = F_1 \Gamma_{xy} \Gamma_{nn}^{(1)} \Lambda_n^{(1)} N_{\text{inv}}$
Inversion	$N_{\text{inv}} = f(\epsilon_q^e, \mu_e, T) + f(\epsilon_q^h, \mu_h, T) - 1$
Frequency locking	$B_{nm} = F_1 \Gamma_{xy} \Gamma_{nm}^{(1)} \Lambda_m^{(1)} N_{\text{inv}}$
Gain compression	$\kappa_{nm} = 2\Gamma_{nm}^{(3)} \gamma \text{Re}(\Lambda_{nm}^{(3)}) / [\Gamma_{nn}^{(1)} \gamma_{\text{ab}} \text{Re}(\Lambda_{nn}^{(1)})]$
Frequency pushing	$\tau_{nm} = 2F_1 \Gamma_{nm}^{(3)} \text{Im}(\Lambda_{nm}^{(3)}) \gamma / \gamma_{\text{ab}}$
Linear mode confinement	$\Gamma_{nn}^{(1)} = N_c^{-1} \int_{z_1}^{z_2} dz n^2(z) u_n(z) u_n(z)$
Nonlinear mode confinement	$\Gamma_{nm}^{(3)} = N_c^{-1} \int_{z_1}^{z_2} dz n^2(z) u_n^2(z) u_m^2(z)$
Linear susceptibility spectral contribution	$\Lambda_n^{(1)} = \sum_q D_\gamma(\Delta_{nq})$ , where $\Delta_{nq} = \Omega_n - \omega_q$
Nonlinear susceptibility spectral contribution	$\Lambda_{nm}^{(3)} = \sum_q D_\gamma(\Delta_{nq}) L_\gamma(\Delta_{nq}) \Lambda_{nm}^{(3)} = \gamma / \gamma_{\text{ab}} \sum_q D_\gamma(\Delta_{nq}) \{2L_\gamma(\Delta_{mq}) + D_{\gamma_{\text{ab}}}(\Omega_n - \Omega_m) [D_\gamma(\Delta_{nq}) + D_\gamma(\Delta_{qm})]\}$

where we assumed that the gain region extends over the entire III–V cavity length. In the above equation,  $\Gamma_{xy}$  is the transverse mode confinement factor for the gain region,  $\wp$  is the dipole matrix element for the interaction between an electron–hole pair and the laser field,  $N_{\text{QD}}^{(2d)}$  is the 2-dimensional QD density in each embedding quantum well (QW) layer of thickness  $h_{\text{QW}}$ . The connection to quantum mechanics is through the Heisenberg operators  $c_q$  and  $b_q$ , which are the electron and hole annihilation operators, respectively. For narrow linewidth lasers, where lasing should involve only the ground-state transition, we use  $q$  to label a group of QDs with the same ground state transition frequency  $\omega_q$ . The  $q$  summation is over the inhomogeneous QD distribution.<sup>[23]</sup>

The laser derivation gives the intensity- and frequency-determining equations for each composite laser/free-space mode,

$$\frac{dI_n}{dt} = [g_n^{\text{sat}}(N^{(2d)}) - \gamma_n^{\text{cav}}] I_n + S_n(N^{(2d)}) + \sum_{m \neq n} 2\sqrt{I_n I_m} \text{Re}[B_{nm}(N^{(2d)}) e^{-i\psi_{nm}}] \quad (11)$$

$$\frac{d\psi_n}{dt} = \Omega_n + \left[ \sigma_n(N^{(2d)}) - \sum_m \tau_{nm}(N^{(2d)}) I_m \right] + iS_n^\phi(N^{(2d)}) + \sum_{m \neq n} \sqrt{\frac{I_m}{I_n}} \text{Im}[B_{nm}(N^{(2d)}) e^{-i\psi_{nm}}] \quad (12)$$

where  $I_n = (\wp E_n / (2\hbar\gamma))^2$  and  $d\psi_n/dt$  are the  $m$ th mode dimensionless intensity and lasing frequency,  $\gamma$  is the dephasing rate and  $\psi_n = v_n t + \phi_n$ . In Equation (11),  $g_n^{\text{sat}}$  is the saturated gain at carrier density  $N^{(2d)}$ ,  $\gamma_n^{\text{cav}}$  is the passive cavity linewidth determined from the absorption  $\alpha(z)$  and the mode confinement factors  $\Gamma_{1,m}^{(1)}$  and  $\Gamma_{2,m}^{(1)}$ . The terms in both equations containing  $\psi_{nm} = \psi_n - \psi_m$  are from the first order polarization, present because the composite-cavity modes are not orthogonal when integrated over only the gain region. They play an important role in the line narrowing of integrated III–V/SiN lasers. Also con-

tributing to line narrowing are the effects of carrier-induced refractive index change (square bracket in Equation (12)). It modifies the passive composite-cavity mode frequency  $\Omega_n$ . In laser theory, they are referred to as the frequency pulling and pushing  $\sigma_n$  and  $\tau_{nm}$ , respectively. In semiconductor laser models, they describe the carrier-induced refractive index change and is typically taken into account via the linewidth enhancement factor.<sup>[24]</sup> Lastly, the spontaneous emission contributions  $S_n$  and  $S_n^\phi$  are incorporated as described in Section 2.3. The purely imaginary contribution  $iS_n^\phi$  describes the dissipation resulting in broadening of each composite-cavity mode making up the quasimode.

In our treatment, all the coefficients associated in Equations (11) and (12) are derived from the electron–hole polarization equation of motion, and are therefore, calculated instead of fitting parameters (see equations in Table 1). More details on the active medium contributions are discussed later, when we explain the line narrowing mechanisms within the context of a laser/free-space composite-cavity mode picture. A difference between a semiconductor laser and an atomic or molecular one is that it cannot be categorized as either homogeneously or inhomogeneously broadened. Owing to rapid carrier–carrier scattering, a semiconductor laser tunes inhomogeneously and saturates homogeneously.<sup>[23]</sup> A consequence is that the intensity- and frequency-determining equations alone do not determine laser behavior. An expedient approach is to evaluate all active medium coefficients at the saturated carrier density  $N_{2d}$ . To do this, Equations (11) and (12) are solved simultaneously with the total carrier density equation of motion:

$$\frac{dN_{2d}}{dt} = \frac{\epsilon_B h_{\text{qw}}}{8\hbar v_0} \left( \frac{\wp}{2\hbar\gamma} \right)^2 \frac{1}{\Gamma_{xy}} \sum_n g_n^{\text{sat}} I_n + \frac{\eta_p J}{eN_{\text{QW}}} - \gamma_{\text{nr}} N_{2d} - B_{\text{spont}}^{(2d)} N_{2d}^2 \quad (13)$$

where  $\epsilon_B$  and  $v_0$  are the averaged permittivity and frequency. For the injection current contributions,  $\eta_p$  is the pump efficiency due to Pauli blocking,  $J$  is the injection current density,  $N_{\text{QW}}$  is the number QW layers with embedded QDs in the active medium. For carrier losses, we use the effective rates,  $\gamma_{\text{nr}}$  for the

nonradiative (Shockley–Read–Hall) carrier loss and  $B_{\text{spont}}^{(2d)}$  for the bimolecular carrier recombination due to spontaneous emission. While there are more detailed treatments,<sup>[23,25]</sup> the above approach has the advantage of reducing numerical demands and yet remaining connected to microscopic details such as bandstructure. Its accuracy depends on laser operation close to quasi-equilibrium condition, which is likely satisfied during narrow linewidth operation.

Assuming quasiequilibrium conditions, the carrier density  $N_{2d}$  gives the occupation in the QD and QW states. The condition

$$\begin{aligned} N_{2d} &= \frac{1}{A} \sum_q f(\epsilon_q^e, \mu_e, T) + \frac{N_{\text{QW}}}{A} \sum_k f(\epsilon_k^e, \mu_e, T) \\ &= \frac{1}{A} \sum_q f(\epsilon_q^h, \mu_h, T) + \frac{N_{\text{QW}}}{A} \sum_k f(\epsilon_k^h, \mu_h, T) \end{aligned} \quad (14)$$

gives the chemical potentials  $\mu_e$  and  $\mu_h$  for the Fermi function

$$f(\epsilon_q^\sigma, \mu_\sigma) = \frac{1}{\exp\left[\left(\epsilon_q^\sigma - \mu_\sigma\right) / \left(k_B T\right)\right] + 1} \quad (15)$$

(with  $o = e$  or  $h$  for electron or hole) used in evaluating the gain medium coefficients in Table 1. In Equations (14) and (15),  $A$  is the active region area, and the electron and hole energies and chemical potentials are relative to their respective QD ground state energies at the centers of the inhomogeneous distributions. Specifically,  $\epsilon_q^\sigma$  is the QD level energy for the  $q$ th group,  $\epsilon_k^\sigma = \Delta_\sigma + \hbar^2 k^2 / (2m_\sigma)$  is the QW carrier energy, the summations are over  $k$  the momentum of the electron or hole QW state, and  $q$  labels the level in the inhomogeneous QD distribution. For the InAs QD structure considered, we use the confinement energies  $\Delta_e = 100$  meV and  $\Delta_h = 65$  meV, and effective masses  $m_e = 0.067 m_0$  and  $m_h = 0.180 m_h$ . With this energy scheme, the QD transition energy is  $\hbar\omega_q = \epsilon_q^e + \epsilon_q^h + \epsilon_g$ , and the chemical potential separation is  $\mu_{\text{eh}} = \mu_e + \mu_h + \epsilon_g$ , where the InAs bandgap energy is  $\epsilon_g = 0.943$  eV.

### 2.3. Connection to Quantum Optics

We close this section with an explanation of how we incorporate the effects of spontaneous emission into our basically semiclassical laser model. From a cavity-QED derivation, we obtain the equation of motion for the single-mode intracavity photon number. Assuming that the electron-hole polarization changes sufficiently fast to follow any time variation in the photon and carrier populations (rate equation approximation and consistent with quasi-equilibrium condition), the polarization may be adiabatically eliminated. In the resulting photon number equation of motion, the spontaneous emission contribution appears explicitly as a bimolecular carrier recombination term.<sup>[26]</sup> Using the conversion,

$$I_n = \left(\frac{\mathcal{G}}{2\hbar\gamma}\right)^2 \frac{\hbar v_n}{\epsilon_B V_{\text{mode}}} n_n \quad (16)$$

we obtain

$$\begin{aligned} S_n &= \frac{\epsilon_g N_{\text{QW}} w L_g}{\epsilon_B V_{\text{mode}}} \left(\frac{\mathcal{G}}{2\hbar\gamma}\right)^2 \Gamma_{\text{nn}}^{(1)} \beta_{\text{spont}} B_{\text{spont}}^{(2d)} N_{2d}^2 f(\epsilon_n^e, \mu_e, T) \\ &\quad \times f(\epsilon_n^h, \mu_h, T) \end{aligned} \quad (17)$$

where  $n_n$  is the photon number in the  $n$ th composite-cavity mode,  $V_{\text{mode}}$  is the composite-mode volume,  $w$  and  $L_g$  are the stripe width and length of the active region,  $\beta_{\text{spont}}$  is the spontaneous emission factor,  $f(\epsilon_n^e, \mu_e, T)$  and  $f(\epsilon_n^h, \mu_h, T)$  are the electron and hole populations (assuming Fermi functions) contributing to the spontaneous emission.

To obtain the spontaneous emission contribution to the frequency determining Equation (12), we derive the equation of motion for the photon annihilation operator in a composite-cavity mode. Working in the Interaction Picture, the equation of motion for the photon annihilation operator in a composite-cavity mode, to 3rd order in light-matter interaction, is<sup>[14]</sup>

$$\frac{dA}{dt} = \left(g - \frac{\gamma_{\text{cav}}}{2}\right) A - \beta AA^\dagger A + G \quad (18)$$

where  $g$  and  $\beta$  are the linear and nonlinear amplitude gain coefficients,  $G$  is the Langevin force operator from spontaneous emission and for brevity, we drop the mode index. Assuming that photon number fluctuation is negligible and  $\langle A(0) \rangle = \sqrt{n_p}$ , we write for the slowly varying photon annihilation operator,

$$\begin{aligned} \langle A(t) \rangle &= \sqrt{n_p} \langle \exp[-i\phi(t)] \rangle, \\ &= \sqrt{n_p} \langle 1 + i\phi(t) - \frac{1}{2}\phi(t)\phi(t) + \dots \rangle \\ &= \sqrt{n_p} \exp[-\langle \phi(t)\phi(t) \rangle / 2] \end{aligned} \quad (19)$$

assuming that the phase noise from spontaneous emission has a Gaussian probability distribution specified by zero mean and second order correlation function with  $\delta$  function time correlation from the Markoff approximation.<sup>[16]</sup> Recalling that we neglect photon number fluctuation, we obtain from Equation (18) the quantum optical contribution to the frequency-determining equation:

$$\frac{d\phi(t)}{dt} = \frac{i}{2\sqrt{n_p}} [G(t) e^{i\phi(t)} - G^\dagger(t) e^{-i\phi(t)}] \quad (20)$$

which we formally integrate and perform more algebra to get

$$\begin{aligned} \langle \phi(t)\phi(t) \rangle &= \frac{1}{4n_p} \int_0^t dt_1 \int_0^t dt_2 \langle G^\dagger(t_1) e^{-i\phi(t_1)} G(t_2) e^{i\phi(t_2)} \\ &\quad + G(t_1) e^{i\phi(t_1)} G^\dagger(t_2) e^{-i\phi(t_2)} \rangle \end{aligned} \quad (21)$$

For the correlations involving the Langevin force operators, we perform a separate lengthy calculation, where we make use of Einstein relation,<sup>[16,27]</sup> to obtain the 2nd order two time Langevin force correlation:

$$\langle G^\dagger(t) G(t') \rangle + \langle G(t') G^\dagger(t) \rangle = 2\gamma_{\text{cav}} \delta(t - t') \quad (22)$$

Equations (21) and (22) give  $\langle \phi(t)\phi(t) \rangle = \gamma_{\text{cav}} t / (2n_p)$ . Hence, to account for phase diffusion due to spontaneous emission, we add to the semiclassical frequency determining equation a damping term,

$$S_n^\phi = \gamma_n^{\text{cav}} \frac{\epsilon_B V_{\text{mode}}}{2\hbar v_n} \left( \frac{\wp}{2\hbar\gamma} \right)^2 \frac{1}{I_n} \quad (23)$$

In reaching Equation (23) we followed the derivation for a two-level system and assume clamping of the gain to the cavity loss rate  $\gamma_{\text{cav}}$ .<sup>[14]</sup> For bulk or QW lasers, more detailed descriptions of the 2nd order two-time Langevin force correlation may be found in the literature.<sup>[28,29]</sup> Work in progress to derive an expression starting with a fully quantized QD laser model.<sup>[30]</sup>

### 3. Intrinsic Linewidth of Integrated III–V/SiN Laser

This section describes application of the approach in Section 2 to study the physical processes occurring when a laser is coupled to a high- $Q$  passive resonator. We consider laser configurations giving the composite-cavity spectra such as in Figure 2b. Furthermore, we assume that an intracavity filter, such as a DBR, is present to enable single quasi (Fox-Li) mode operation. For the active region, we use a design that has performed very well in experiments.<sup>[31]</sup> It consists of 5  $\text{In}_{0.15}\text{Ga}_{0.85}\text{As}$  QWs, each 7 nm thick and embedding a density of  $2 \times 10^{10} \text{ cm}^{-2}$  InAs QDs. From electronic structure calculations, the dipole matrix element  $\wp = e \times 0.6 \text{ nm}$  and ground-state transition energy is  $\hbar \omega_0 = 0.943 \text{ eV}$ . Base on quantum kinetic calculations and single-section laser measurements,<sup>[32]</sup> we use  $\gamma = 2 \times 10^{12} \text{ s}^{-1}$  for the dephasing rate,  $\gamma_{\text{ab}} = 10^{11} \text{ s}^{-1}$  and  $\gamma_{\text{nr}} = 10^9 \text{ s}^{-1}$  for the inter-QD population relaxation and nonradiative decay rates, respectively, carrier injection efficiency  $\eta = 0.35$  and QD inhomogeneous broadening  $\Delta_{\text{inh}} = 15 \text{ meV}$ .<sup>[33,34]</sup>

To obtain the results in this section, we first solve Equation (3) with boundary conditions Equations (4)–(6) for the composite-cavity mode frequencies and eigenfunctions. Using the latter, we compute the mode confinement and overlap factors  $\Gamma_{\text{nm}}^{(1)}$  and  $\Gamma_{\text{nm}}^{(3)}$  for evaluating the laser coefficients in Table 1. A typical quasi-mode (Fox-Li) resonance consists of a few hundred composite-cavity modes. The mode intensities and lasing frequencies are determined by intensity- and frequency-determining Equations (11) and (12). We numerically solve the coupled Equations (11)–(13) until steady state is reached and compute the output power and lasing spectrum for a given current:

$$P = \gamma_{\text{out}} \frac{1}{4} \epsilon_B V_{\text{mode}} \left( \frac{\wp}{2\hbar\gamma} \right)^{-2} \sum_n \Gamma_{\text{nn}}^{(2)} I_n \quad (24)$$

$$S(\Delta f) = \frac{1}{T} \int_t^{t+T} dt_1 \int_0^\infty d\tau E_{\text{tot}}(t_1 + \tau) E_{\text{tot}}(t_1) e^{i2\pi\Delta f\tau} \quad (25)$$

where

$$\begin{aligned} \gamma_{\text{out}} &= -c \ln(1 - T_2) / (2L_2 n_2) \\ \text{and} \\ E_{\text{tot}}(t) &= \sum_n \sqrt{I_n(t)} \exp[i\psi_n(t)] \end{aligned} \quad (26)$$

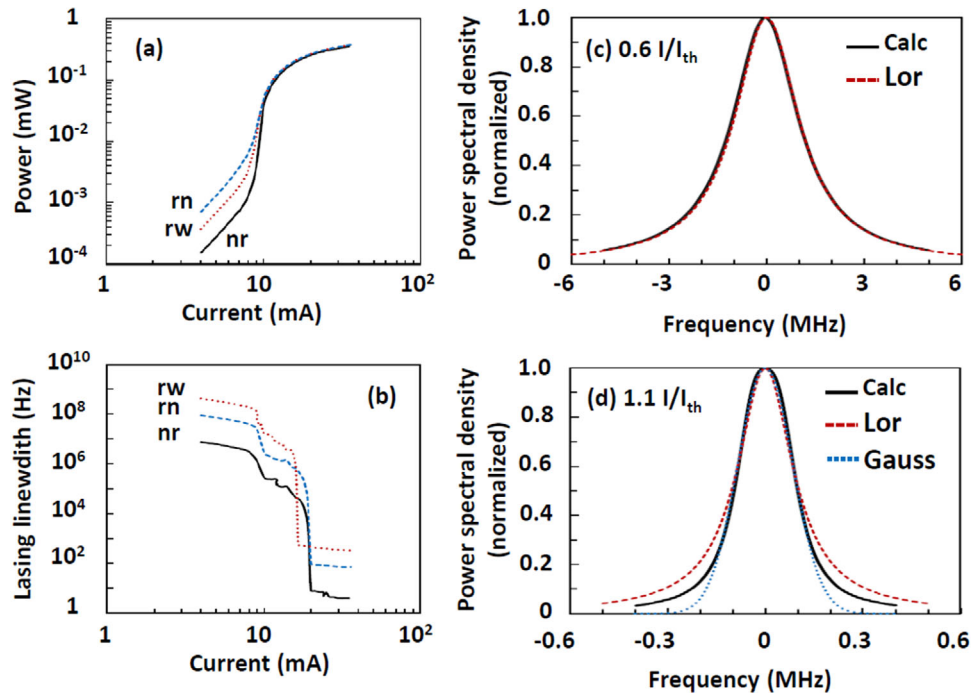
To use Equation (25), we first integrate the laser Equations (11)–(13) until time  $t$ , when the modal intensities reach steady state. Each  $d\tau$  integration gives a lasing spectrum. Then, we repeat the process for different times  $t_1$  to obtain a distribution of lasing spectra. From the time averaged spectrum we extract the lasing linewidth.

Figure 3a,b shows the computed injection current dependences of output power and lasing linewidth for three composite-cavity modes. The light–current ( $L$ – $I$ ) curves are essentially similar for both resonant and non-resonant configurations. Displacements of the linewidth curves are according to the width of the passive composite-cavity mode resonances. However, their shapes are similar and indicate that spectral narrowing occurs in two stages. From the onset of lasing to twice the threshold, there is already appreciable stimulated emission occurring to produce noticeable narrowing of the spontaneous emission spectrum. The linewidth decreases from the passive cavity value with increasing intracavity intensity from gain clamping or narrowing, as in single-Fabry Perot or distributed feedback (DFB) lasers. At excitations above twice the lasing threshold, a behavior unique to coupled cavities comes into play. There is a drastic further decrease in linewidth caused by frequency locking of composite-cavity modes. The mechanism involves the term containing the relative phase  $\psi_{\text{nm}}$  in Equation (12). With higher injection current, the linewidth settles to a value solely determined by  $S_n^\phi$  in Equation (23).

The simulations uncover two interesting features of the emission spectra during the transition to narrow linewidth operation. One is a change in spectral shape from below to above lasing threshold. Below threshold, the entire amplified spontaneous emission spectrum is exactly a Lorentzian function (Figure 3c). Above the lasing threshold, the lineshape deviates from the Lorentzian function (compare black solid and red dashed curves in Figure 3d). The blue dotted curves suggest a better fit to a Gaussian function down to about 20% of the spectral peak. This lineshape change has been reported earlier.<sup>[35,36]</sup> A quantum optical calculation using a quasi-mode description of out-coupling, is unable to describe the new shape. In the present picture, the slightly flatter shape close to the spectral peak and the sharper drop at the spectral tails come from partial locking of the composite-cavity modes.

The partially locked regime is the second interesting feature. For a closer examination, we monitor time dependences of the lasing frequency  $d\psi_n/dt$  for the three composite-cavity modes indicated in Figure 4a. In the absence of locking, one has a straight line with unity slope. Deviation, as depicted by the dashed curve, indicates the onset of frequency locking. When completely locked, one has a flat line with zero slope. Figure 4b shows that the lasing frequencies are mostly tightly bunched, except when interrupted by spikes. Earlier reports have associated the spikes with dark solitons.<sup>[37,38]</sup> Comparison of Figure 4b,c for  $I = 10 \text{ mA}$  and  $I = 15 \text{ mA}$  shows an increased period between spikes. This results in narrower average linewidth from the  $dt_1$  integration in Equation (25). For  $I = 20 \text{ mA}$ , stable, complete locking occurs, the spikes vanish and one has the narrowest achievable lasing spectrum that reverts to a Lorentzian lineshape.

In the composite-cavity mode picture, the spikes are instances of coherence collapse when the system breaks lock. The top inset in Figure 4b shows the coherence collapse region in greater



**Figure 3.** Calculated a) output power and b) linewidth (full width at half maximum) versus injection current. The effective coupling between III-V and SiN sections is  $T_1 = 0.02$  and the curves are for the composite-cavity modes (nr, rn, and rw) as indicated. Emission spectra from III-V/SiN laser c) and d) above lasing threshold, respectively. The black curves are calculated, the red dashed and blue dotted curves are the fits using Lorentzian and Gaussian functions, respectively. The spectra are for the nr mode.

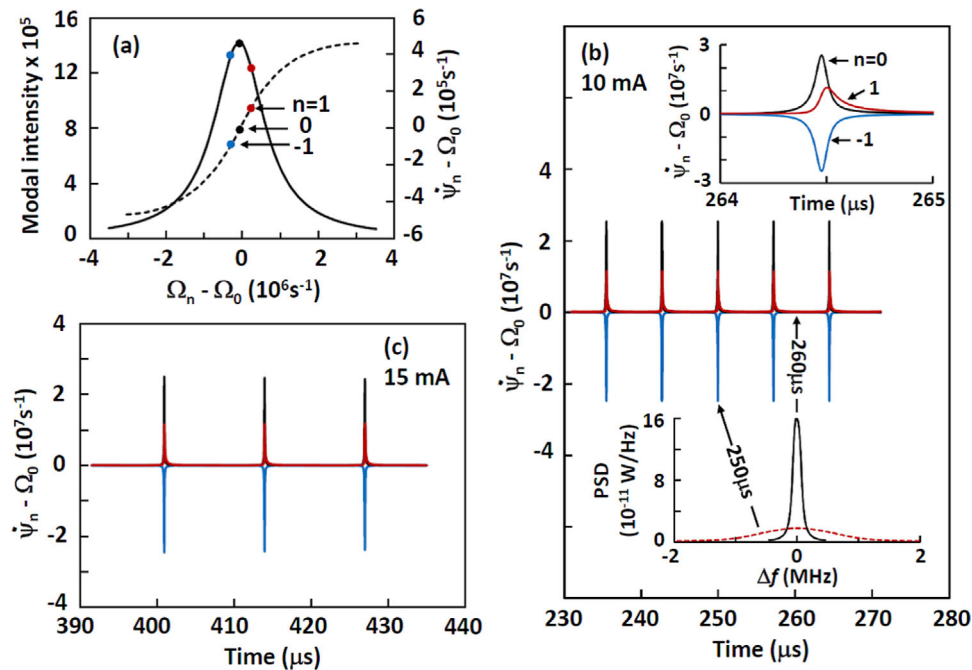


**Figure 4.** a) Modal intensity and lasing frequency (solid and dashed curves, respectively) versus passive composite-cavity frequency after reaching steady-state with 10 mA injection current. The frequencies are relative to  $\Omega_0$ , the frequency at the quasi-mode peak. The points indicate the modal frequencies whose time dependences are tracked. We label those modes (from left to right)  $n = -1, 0$  and 1. b) Time dependences of tracked modal frequencies at 10 mA. The top inset shows higher resolution of the coherence collapse. The bottom inset shows laser spectra at coherence collapse (250  $\mu$ s) and during narrow linewidth operation (260  $\mu$ s). c) The time dependences of tracked modal frequencies at 15 mA.

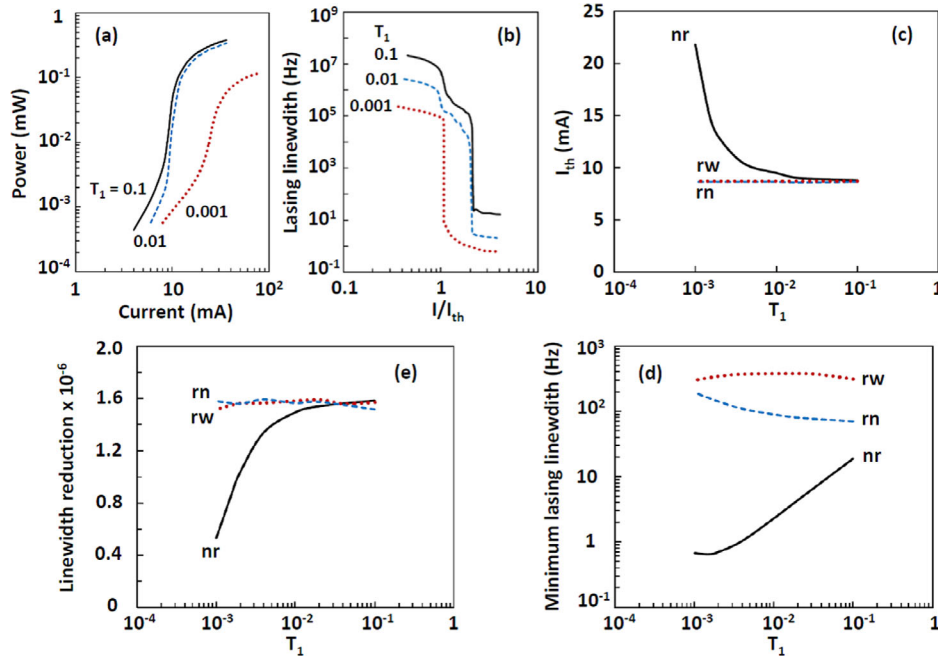


**Figure 5.** a)  $L$ – $I$  and b) FWHM versus excitation for non-resonant (nr) configuration and effective coupling between III–V and SiN sections as indicated. c) Threshold current versus effective coupling between III–V and SiN sections.  $T_1$  is an effective transmission representing the interfacial or evanescent coupling between III–V laser and high- $Q$  SiN cavity. d) Minimum lasing linewidth versus effective coupling between III–V and SiN sections. e) Maximum lasing linewidth reduction versus effective III–V/SiN optical coupling. For d,e),  $I/I_{th} = 3$  where the lasing composite-cavity modes are fully locked. The curves in (c)–(e) are for non-resonant (black solid) and resonant wide (red dotted) and resonant narrow (blue dashed) configurations. e) Summarizes the combined effects of cavity  $Q$  and optical coupling on the minimum achievable laser linewidth. Plotted is the linewidth reduction (SiN cavity linewidth/laser linewidth) versus optical coupling for resonant and non-resonant operation. The calculations are performed for 3 times threshold current to ensure complete locking of the lasing composite-cavity modes, so as to have the maximum linewidth reduction. For the non-resonant (nr) case, the simulations show a relatively constant, large reduction of  $\approx 1.5 \times 10^6$  for  $T_1 > 0.01$  (black solid curve). For smaller  $T_1$ , the curve shows the detrimental effect of too little III–V/SiN coupling, resulting in a sharp drop in linewidth reduction. The curves for the resonant (rn and rw) cases show independence of linewidth reduction on III–V/SiN optical coupling. The reason is that resonant operation is always strongly coupled regardless of optical coupling. Factored into the results of Figure 5e is that when coupled to the III–V laser cavity, the SiN cavity  $Q$  factor varies nonlinearly with  $T_1$ . As an indication, at  $T_1 = 0.1$ , the SiN cavity  $Q$  factors for the nr, rn, and rw configurations are  $7.2 \times 10^6$ ,  $1.96 \times 10^7$ , and  $4.4 \times 10^5$ , respectively. At  $T_1 = 0.01$ , the corresponding SiN cavity  $Q$  factors are  $6.3 \times 10^7$ ,  $1.53 \times 10^6$ , and  $3.6 \times 10^5$ . At  $T_1 = 0.001$ , the corresponding SiN cavity  $Q$  factors are  $6.1 \times 10^8$ ,  $7.0 \times 10^5$ , and  $4.7 \times 10^5$ .

detail. The  $n = 0$  trace indicates a blue shift of the entire spectrum by roughly 4 MHz, and the greater separation between traces indicates significant spectral broadening. This is clearly evident in the bottom inset, where we plot the spectra between spikes and close to the spike maximum (black solid and red dashed curves, respectively). The coherence collapse behavior may be described by Adler’s equation,  $d\psi/dt = a + b\sin(\psi)$ , when  $b \gtrsim a$ , i.e., operation just outside the lockband. As  $b$  increases, the duration between spikes increases as shown in Figure 4b,c. The duration of the spikes also decreases. The average spectral width (averaged over several pike periods) then further decreases, until complete frequency locking is reached and coherence collapse disappears completely.

When formulating our theory, we made sure that it is suitable for parametric studies to produce timely results that are useful for engineering design. We will demonstrate this by presenting results from a parametric study on the effects of optical coupling between III–V and SiN sections. The experimental implementations of coupling include quantum-well intermixing and evanescent field coupling. For the present study, we use the effective transmission  $T_1$  as a measure of the net coupling effect. As in an experiment, varying the optical coupling also alters the passive

cavity linewidths, the most important being that of the high- $Q$  SiN cavity. In the parametric study, we vary  $T_1$  to investigate the competing effects of cavity- $Q$  increase and optical coupling decrease with decreasing optical coupling.

Figure 5a,b show the results for operating with different optical coupling for the non-resonant (nr) mode. Simulations indicate little change in  $L$ – $I$  behavior until  $T_1$  reduces below 0.01. After which, mode confinement factor reduction leads to significant degradation in  $L$ – $I$  behavior, as shown in Figure 5a by the red dotted curve for  $T_1 = 0.001$ . In Figure 5b, we plot the FWHM of the lasing spectrum versus injection current relative to the threshold value. The vertical displacement of the curves indicates the linewidth narrowing from increasing passive SiN cavity  $Q$ . For  $T_1 \geq 0.01$ , spectral narrowing takes place in two stages as discussed earlier. With further decrease in coupling, there is a gradual merging of the gain narrowing and frequency locking stages, that eventually results in a single abrupt drop in lasing linewidth as depicted by the  $T_1 = 0.001$  curve.

The above calculations are repeated for the resonant modes (rn and rw). We operate the laser at  $I/I_{th} = 3$ , which is sufficiently high to fully frequency lock the lasing composite-cavity modes, thus giving the minimum possible linewidth. Figure 5c shows



the dependences of threshold current on III–V/SiN coupling. The increase in threshold current with decreasing coupling for the non-resonant (nr) mode is from the decrease in mode confinement factor in the III–V cavity, consistent with Figure 5a. For the resonant modes there is no change in threshold current because two identical oscillators are always strongly coupled regardless of the coupling. Figure 5d indicates a decreasing laser linewidth with decreasing  $T_1$ , because of increasing SiN cavity  $Q$ , consistent with Figure 5b. At  $T_1 = 0.002$ , the linewidth narrowing saturates, when the increase in SiN cavity  $Q$  is balanced by the decrease in III–V/SiN coupling. Figure 5d also indicates that the dependence of linewidth on III–V/SiN optical coupling is vanishing small, in comparison, for the resonant modes (rn and rw). Again, the reason is that for the resonant modes the III–V and SiN cavities are always strongly coupled.

#### 4. Conclusion

This paper describes a theoretical approach to investigate the linewidth narrowing when a semiconductor quantum-dot laser is optically coupled to a high- $Q$  silicon nitride resonator. The approach uses composite-cavity eigenmodes to treat the III–V laser, passive SiN resonator and free-space as one combined system. There are two advantages. One is validity for arbitrary optical coupling between III–V and SiN sections (from completely isolated to totally coupled). Second is a consistent treatment of outcoupling, which enables the derivation of the laser equations to be more rigorous than possible with the customary one using quasi (non-normal) cavity modes. The description of the active medium follows multimode semiclassical laser theory, where electron–hole polarization dynamics accounts for both linear gain and carrier-induced refractive index change, as well as nonlinearities giving rise to saturation, mode competition and multiwave mixing. Quantum optical contributions are incorporated via a Langevin approach, with modifications to deal with the added complication of having a complex resonator geometry and coupling to free space.

Application of the approach identifies two physical processes underlying linewidth reduction. One is the gain clamping as is the case in single-cavity lasers. The second mechanism (unique to coupled cavities) is frequency locking of composite-cavity modes. Both mechanisms combine to describe details of emission spectra from below to above lasing threshold, such as deviation from a Lorentzian lineshape after the onset of lasing, as observed in experiments. Also described is coherence collapse because of incomplete frequency locking of composite-cavity modes. The periodic occurrences of coherence collapse may correspond to the experimentally observed periodic dips in intensity in heterogeneously integrated III–V/SiN lasers.

Parametric studies suggest the possibility of laser linewidth reduction by six orders of magnitude from that of the high- $Q$  passive cavity. We presented results showing width (FWHM) of 0.6 Hz with SiN cavity  $Q = 6 \times 10^7$ . The parametric studies also indicate the role of the optical coupling between III–V and SiN sections. Preliminary results suggest that the interdependence of the optical coupling and passive-cavity  $Q$  places a limit on the minimum intrinsic linewidth achievable through increasing the passive cavity  $Q$ -factor.

Lastly, the present formulation provides the basis of more detailed models for analyzing experiments and optimizing device engineering. An improvement is to use composite-cavity modes exactly for 2-D device geometries and model precisely the gratings and intermixing regions. In terms of laser theory, the strong signal treatment has room for greater rigor. Lastly, one should examine if there are consistency issues with our incorporation of quantum optical effects into a basically semiclassical laser theory. Given the goal of an analytical tool for engineering integrated III–V/SiN lasers, improvements should be introduced without increasing numerical complexity to the point of making parametric studies impractical. In fact, there is motivation for reducing the complexity of the present equations. The reason is so that bifurcation-continuation techniques may be used to systematically and extensively analyze the rich nonlinear dynamics found in closely resonant, very weakly coupled oscillators (in our case rn and rw operation for  $T_1 < 0.001$ ).<sup>[39,40]</sup> The next series of investigations will concentrate on high coherence lasers made with harmonic potential. Such complex semiconductor QW or QD lasers heterogeneously integrated with silicon photonics exhibit a large cavity  $Q$ , indicating their vast potential for optical radars, on-chip atomic clocks, and future coherent technologies.

#### Acknowledgements

This work was supported by Advanced Research Projects Agency-Energy (ARPA-E) No. DE-AR000067, the U.S. Department of Energy under Contract No. DE-AC04-94AL85000, and the American Institute for Manufacturing (AIM) Integrated Photonics. This work was performed, in part, at the Center for Integrated Nanotechnologies, an Office of Science User Facility operated for the U.S. Department of Energy (DOE) Office of Science. The authors thank C. Shen, L. Chang, and M. Gehl for discussions.

#### Conflict of Interest

The authors declare no conflict of interest.

#### Data Availability Statement

The data that support the findings of this study are available from the corresponding author upon reasonable request.

#### Keywords

linewidth narrowing, multimode laser theory, quantum-dot lasers | heterogeneous III-V/Si integration

Received: October 29, 2021

Revised: February 21, 2022

Published online:

- [1] M. A. Tran, D. Huang, J. E. Bowers, *APL Photonics* **2019**, *4*, 111101.
- [2] M. Matthews, K. Cameron, R. Wyatt, W. Devlin, *Electron. Lett.* **1985**, *21*, 113.
- [3] M. Okai, M. Suzuki, T. Taniwatari, N. Chinone, *Jpn. J. Appl. Phys.* **1994**, *33*, 2563.

- [4] Z. Zhang, J. Liu, J. Guo, H. Yuan, J. Bai, N. Zhu, in *Asia Communications and Photonics Conference*, Shanghai, November, **2015**, AM1B-3.
- [5] B. Kelly, R. Phelan, D. Jones, C. Herbert, J. O'Carroll, J. Rensing, J. Wendelboe, J. Watts, A. Kaszubowska-Anandarajah, P. Perry, C. Guignard, *Electron. Lett.* **2007**, 43.
- [6] N. Pourshab, A. Gholami, M. J. Hekmat, N. Shahriyari, *J. Opt. Soc. Am. B* **2017**, 34, 2414.
- [7] T. Septon, A. Becker, S. Gosh, G. Shtendel, V. Sichkovskiy, F. Schnabel, A. Sengül, M. Bjelica, B. Witzigmann, J. P. Reithmaier, G. Eisenstein, *Optica* **2019**, 6, 1071.
- [8] A. Becker, V. Sichkovskiy, M. Bjelica, A. Rippien, F. Schnabel, M. Kaiser, B. Witzigmann, G. Eisenstein, J. Reithmaier, *Appl. Phys. Lett.* **2017**, 110, 181103.
- [9] C. T. Santis, Y. Vilenchik, N. Satyan, G. Rakuliic, A. Yariv, *Proc. Natl. Acad. Sci. U. S. A.* **2018**, 115, E7896.
- [10] A. Gallet, K. Hassan, C. Jany, T. Card, J. Da Fonseca, V. Rebeyrol, A. Shen, J. Provost, F. Van Dijk, N. Girard, V. Muffato, in *IEEE International Semiconductor Laser Conference*, Sante Fe, September, **2018**, pp. 1–2
- [11] W. Jin, Q. - F. Yang, L. Chang, B. Shen, H. Wang, M. A. Leal, L. Wu, M. Gao, A. Feshali, M. Paniccia, K. J. Vahala, J. E. Bowers, *Nat. Photonics* **2021**, 15, 346.
- [12] S. A. Shakir, W. W. Chow, *Opt. Lett.* **1984**, 9, 202.
- [13] A. E. Siegman, *Lasers University Science Books*, Mill Valley, CA **1986**, vol. 37, p. 169.
- [14] M. Sargent, III, M. O. Scully, W. E. Lamb, Jr, *Laser Physics*, Addison-Wesley, Reading **1974**.
- [15] W. W. Chow, F. Jahnke, C. Gies, *Light: Sci. Appl.* **2014**, 3, e201.
- [16] M. Lax, *Phys. Rev.* **1966**, 145, 110.
- [17] K. J. Ebeling, L. A. Coldren, *J. Appl. Phys.* **1983**, 54, 2962.
- [18] W. T. Tsang, N. A. Olsson, *Appl. Phys. Lett.* **1983**, 43, 527.
- [19] W. W. Chow, Z. S. Yang, G. A. Vawter, E. J. Skogen, *IEEE Photonics Technol. Lett.* **2009**, 21, 838.
- [20] W. W. Chow, *Phys. Rev. A* **2006**, 73, 013821.
- [21] R. Lang, M. O. Scully, W. E. Lamb, Jr., *Phys. Rev. A* **1973**, 7, 1788.
- [22] M. B. Spencer, W. E. Lamb, Jr., *Phys. Rev. A* **1972**, 5, 884.
- [23] W. W. Chow, S. W. Koch, *IEEE J. Quantum Electron.* **2005**, 41, 495.
- [24] C. H. Henry, *IEEE J. Quantum Electron.* **1982**, 18, 259.
- [25] I. Waldmueller, W. W. Chow, M. C. Wanke, E. W. Young, *IEEE J. Quantum Electron.* **2006**, 42, 292.
- [26] W. W. Chow, S. Reitzenstein, *Appl. Phys. Rev.* **2018**, 5, 041302.
- [27] W. W. Chow, "Fluctuation phenomena in quantum optics," University of Arizona, Tucson, 1975 (available at azu\_td\_7602537\_sip1\_m.pdf).
- [28] G. Lasher, F. Stern, *Phys. Rev.* **1964**, 133, A553.
- [29] H. Wenzel, M. Kanter, M. Radziunas, U. Bandelow, "Semiconductor laser linewidth theory revisited," *arXiv:2105.00535v2 [physics.optics]* 5 June 2021.
- [30] S. Ates, C. Gies, S. M. Ulrich, J. Wiersig, S. Reitzenstein, A. Löffler, A. Forchel, F. Jahnke, P. Michler, *Phys. Rev. B* **2008**, 78, 155319.
- [31] S. Liu, D. Jung, J. C. Norman, M. J. Kennedy, A. C. Gossard, J. E. Bowers, *Electron. Lett.* **2018**, 54, 432.
- [32] W. W. Chow, F. Jahnke, *Prog. Quantum Electron.* **2013**, 37, 109.
- [33] J. C. Norman, D. Jung, Z. Zhang, Y. Wan, S. Liu, C. Shang, R. W. Herrick, W. W. Chow, A. C. Gossard, J. E. Bowers, *IEEE J. Quantum Electron.* **2019**, 55, 200511.
- [34] T. Septon, A. Becker, S. Gosh, G. Shtendel, V. Sichkovskiy, F. Schnabel, A. Sengül, M. Bjelica, B. Witzigmann, J. P. Reithmaier, G. Eisenstein, *Optica* **2019**, 6, 1071.
- [35] L. D. Mercer, *J. Lightwave Technol.* **1991**, 9, 485.
- [36] G. M. Stephan, T. T. Tam, S. Blin, P. Bernard, M. Tetu, *Phys. Rev. A* **2005**, 71, 043809.
- [37] G. R. Allan, S. R. Skinner, D. R. Andersen, A. L. Smirl, *Opt. Lett.* **1991**, 16, 156.
- [38] L. A. Lugiato, R. Lefever, *Phys. Rev. Lett.* **1987**, 58, 2209.
- [39] S. Wieczorek, W. W. Chow, *Opt. Commun.* **2005**, 246, 471.
- [40] S. Wieczorek, W. W. Chow, *Phys. Rev. Lett.* **2004**, 92, 213901.